MOSAIC: Mask Optimizing Solution With Process Window Aware Inverse Correction

Jhih-Rong Gao, Xiaoqing Xu, Bei Yu, and David Z. Pan
ECE Dept. Univ. of Texas at Austin, Austin, TX 78712
{ jrgao, xiaoqingxu, bei, dpan}@cerc.utexas.edu

ABSTRACT

Optical Proximity Correction (OPC) has been widely adopted for resolution enhancement to achieve nanolithography. However, conventional rule-based and model-based OPCs encounter severe difficulties at advanced technology nodes. Inverse Lithography Technique (ILT) that solves the inverse problem of the imaging system becomes a promising solution for OPC. In this paper, we consider simultaneously 1) the design target optimization under nominal process condition and 2) process window minimization with different process corners, and solve the mask optimization problem based on ILT. The proposed method is tested on 32nm designs released by IBM for the ICCAD 2013 contest. Our optimization is implemented in two modes, MOSAIC_fast and MOSAIC_exact, which outperform the first place winner of the ICCAD 2013 contest by 7% and 11%, respectively.

1. INTRODUCTION

As technology nodes continue shrinking, semiconductor industry is still stuck at 193nm lithography. Due to the resolution limit, various resolution enhancement techniques (RETs) have been proposed to achieve deep sub-wavelength lithography. Optical Proximity Correction (OPC) is one of the RETs that have been widely used.

Typical OPC approaches can be divided into two categories: rule-based approach [1] and forward model-based approach [2]. Rule-based OPC is simple and fast, but only suitable for less aggressive designs. Forward model-based OPC usually relies on edge fragmentation and movement, where mask is adjusted iteratively based on mathematical models. To allow more flexibility, a topological invariant pixel based OPC [3] was proposed. However, the solution space of these approaches is natively limited and thus OPC in advance technology nodes has become more challenging. Inverse models-based method, also referred as Inverse lithography technique (ILT) [4, 5], is one of the strong OPC candidates for 32nm and beyond [6].

ILT-based OPC solves the inverse problem of the imaging system through optimizing an objective function. The ILT process starts from the target printed patterns and iteratively optimizes the mask. ILT approaches are expected to achieve better results than conventional OPC methods be-

cause its pixelated mask optimization enables better contour fidelity.

In recent years, ILT has drawn more attention because of its great flexibility in mask optimization. Granik [7] proposed a fast solution based on constrained nonlinear formulation. Shen et al. [8] formulated ILT as a nonlinear image restoration problem, and solved it by a level-set time-dependent model. Poonawala et al. [9] formulated the inverse problem as a continuous function and optimized the mask by the gradient descent approach. Various enhancement techniques [10–12] have been presented based on the gradient descent framework. Zhang et al. proposed cost function reduction methods [13, 14] to make the optimization less dependent on the initial condition. However, most of these approaches only optimized image contour, and only [11] considered the focus variation. Moreover, none of them can directly optimize edge placement error (EPE), which is an important measurement for yield impact.

The main objective for OPC is to obtain an optimized mask that can compensate the pattern distortion. However, as the feature size is getting smaller, the yield impact of layout uncertainty during the manufacturing process is getting larger. Considering manufacturing variability has thus become an important issue for mask optimization and has been studied in several forward model-based OPC methods [15–17]. In order to tackle the above issues in ILT, in this paper, we propose new mask optimization approaches considering simultaneously 1) the design target optimization under nominal process condition and 2) process window minimization with different process corners. The main contributions include:

- We propose mask optimizing approaches considering design target and process window simultaneously.

- We formulate the EPE violation as a sigmoid function and derive the closed form of its gradient for EPE minimization.

- We present MOSAIC_exact that achieves the best results among all compared approaches, and MOSAIC_fast with efficient gradient computation.

- We perform experiments on 32nm M1 designs released by IBM and show that our two approaches outperform the first place winner of the ICCAD 2013 contest by 7% and 11%, respectively.

The rest of the paper is organized as follows. We first give an introduction of the forward lithography process in Sec. 2. Our mask optimization approaches are explained in Sec. 3. Finally, we show our experimental results and comparison in Sec. 4, followed by the conclusion in Sec. 5.
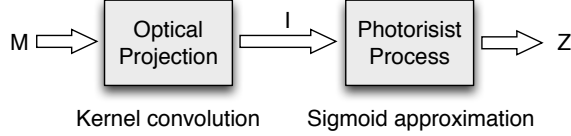
Table 1: Variable and symbol definitions.

Variables	Definitions
M	Mask
I	Intensity after optical system
Z	Printed pattern after photoresist process
N	Length/Width of the mask
$\otimes$	Convolution operator
$\odot$	Element-by-element multiplication

Figure 1: Forward lithography process model.

2. FORWARD LITHOGRAPHY

We first explain the mathematical form of the forward lithograph process. Table 1 gives the basic variables and operators. The lithography process is shown as Fig. 1. The mask M is projected through optical lens onto the wafer plane, which is coated with photoresist. The aerial image I then goes through development and etching processes to form the final printed image Z. The forward lithography process of obtaining printed image from a given mask can be modeled with two phases, optical projection model and photoresist model.

The Hopskins diffraction model [18] has been widely used for partially coherent imaging system. To reduce the computational complexity, we adopt the singular value decomposition model (SVD) [19] to approximate the Hopskins model in this paper. In SVD model, the Hopskins diffraction model can be decomposed into a sum of coherent systems based on eigenvalue decomposition as Eq. (1).

$$I(x,y) = \sum_{k=1}^{N^2} w_k |M(x,y) \otimes h_k(x,y)|^2, \quad x,y = 1,2,...N \quad (1)$$

where h_k is the kth kernel of the model and w_k is the corresponding weight of the coherent system. The N_hth order approximation to the partially coherent system can be obtained by

$$I(x,y) \approx \sum_{k=1}^{N_h} w_k |M(x,y) \otimes h_k(x,y)|^2. \quad (2)$$

In our implementation, the system is approximated with $N_h = 24$ kernels.

The light transmitted through the mask is then exposed on the photoresist. An image can be developed if the light intensity of the exposed area exceeds a threshold th_r. Therefore, the photoresist effect can be defined by the following step function:

$$Z(x,y) = \begin{cases} 0 & \text{if } I(x,y) \leqslant th_r \\ 1 & \text{if } I(x,y) > th_r \end{cases} \quad (3)$$

Later in this paper, we will derive the partial differential of the imaging system. In order to obtain a continuous form, we apply the sigmoid function to approximate the threshold
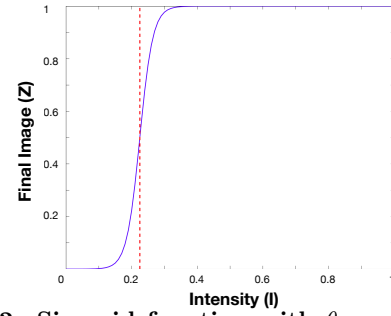
Figure 2: Sigmoid function with $\theta_Z = 50$ and $th_r = 0.225$.

model:

$$Z(x,y) = sig(I(x,y)) = \frac{1}{1+e^{-\theta_Z(I(x,y)-th_r)}} \quad (4)$$

where θ_Z defines the steepness of the sigmoid function. Fig. 2 illustrates our sigmoid function with $\theta_Z = 50$ and $th_r = 0.225$.

3. MASK OPTIMIZATION FOR DESIGN TARGET AND PROCESS WINDOW

3.1 Inverse Lithography Based on Gradient Descent

The forward lithography process in Eq. (4) can be described below:

$$Z = f(M) \quad (5)$$

The OPC problem by inverse lithography tries to find:

$$M_{opt} = f^{-1}(Z_t) \quad (6)$$

where Z_t is the target pattern and M_{opt} is the optimized mask with OPC. However, this is an ill-posed problem because different masks may yield the same result. Therefore, there is no directed closed form solution to Eq. (6). Instead, gradient descent based approaches have been commonly used to solve the ILT problem.

The details of our methodologies to solve the ILT problem are shown in Alg. 1. The ILT problem is formulated as a multivariable objective function F where each variable $p(x,y) \in P$ corresponds to a pixel of the mask. As explained previously, our objective in this work is to optimize the design target and the process window, represented and evaluated below.

Minimize: $F = \alpha \times \#EPE\ Violation + \beta \times PV\ Band$
Subject to: $M(x,y) \in \{0,1\}$

$$(7)$$

Algorithm 1

1: $F \leftarrow$ objective function of OPC
2: $M \leftarrow Z_t$ with rule-based SRAF
3: $P \leftarrow$ initialize unconstrained variables corresponding to M
4: **repeat**
5:     $\mathbf{g} \leftarrow$ calculate gradient ∇F
6:     $P \leftarrow P - stepSize \times \mathbf{g}$
7:     $M \leftarrow$ recalculate pixel value based on P
8: **until** $\#iteration = th_{iter}$ or $RMS(g) < th_g$
9: $M_{opt} \leftarrow M^{iter}$ with the lowest objective value

---

where α and β are user-defined parameters to control the tradeoff between the two terms. Edge placement error (EPE) measures the manufacturing distortion by the difference of edge placement between the final image and the target image under nominal process condition. EPE may cause yield impact if its value is larger then a certain threshold th_{epe} and this is referred to as a violation. Process variability band (PV Band) [20] measures the layout sensitivity to process variations, which indicates a range of feature edge placement among possible lithography process variations.

When the gradient descent algorithm is applied, the solution converges to the local optimum of the objective function closest to the initial condition. Starting from a good initial solution gives us a better chance to obtain a good result. An intuitive initial solution is the target mask. Instead of using the target mask directly, we apply simple rule-based OPC [21] by adding sub-resolution assist features (SRAF) in line 2.

Because the mask M contains only binary values, the ILT problem is an integer nonlinear problem and difficult to solve. It is common to relax the binary constraint to convert the ILT problem into an unconstrained optimization problem. We adopt the sigmoid transformation [12] as Eq. (8), which has been shown to provide effective solution searching for gradient descent:

$$M = sig(P) = \frac{1}{1+e^{-\theta_M \cdot P}} \quad , \theta_M: \text{steepness.} \quad (8)$$

The relaxed variable P is therefore unbounded. Line 3 and line 7 in Alg. 1 perform the variable transformation based on the above definition.

In our gradient descent, we start from an initial mask solution and iteratively approach the optimum solution in the direction of the negative gradient of F with the number proportional to $stepSize$ (line 6). In order to directly calculate the gradient, F must be a differentiable function. We will discuss in Sec. 3.2~3.4 how to define F properly and derive the closed form of its gradient. The optimization is repeated until an user-defined iteration threshold th_{iter} is reached or the solution converges to a local optimum. The local optimum can be determined when the gradient becomes zero. Since each pixel inside the mask has its own gradient, we calculate the root mean square (RMS) of gradients of all pixels and exit the loop when it is less then a tolerance value th_g. We further improve the solution quality by exploring multiple local minima. Our implementation integrates the jump technique [12], where the step size will be adjusted to encourage searching the solution from different local minima.

3.2 Design Target Formulation Based on EPE

In this section, we focus on the first half part of Eq. (7) for design target optimization. Although EPE is a common criterion to evaluate image contour, none of existed ILT approaches optimize EPE directly. Here, we propose an exact objective formulation for EPE minimization. Fig. 3 (a) gives an example of how EPE is measured. Measured points are sampled along the boundary of the target patterns, which includes a set of samples on horizontal edges (HS) and a set of samples on vertical edges (VS). We observe that the image distortion is continuous, producing either inner image edges or outer image edges as shown in Fig. 3 (b). Therefore, we can sum up the image difference as $Dsum$ within the range of the EPE constraint th_{epe}. The mathematical form is defined by Eq. (9).
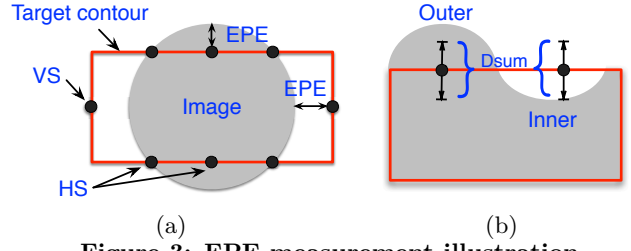

Figure 3: EPE measurement illustration.

$$Dsum_{i,j} = \sum_{k=j-th_{epe}}^{j+th_{epe}} D_{ik} \quad , \text{if } (i,j) \in HS$$

$$Dsum_{i,j} = \sum_{k=i-th_{epe}}^{i+th_{epe}} D_{kj} \quad , \text{if } (i,j) \in VS \quad (9)$$

where

$$D = (Z_{nom} - Z_t)^2 \quad (10)$$

We can then determine if there is an EPE violation based on Eq. (11). Again, since we need to formulate a differentiable equation, this threshold model is approximated by the sigmoid function with a steepness of θ_{epe}.

$$\text{EPE Violation} = \begin{cases} 0 & \text{if } Dsum < th_{epe} \\ 1 & \text{if } Dsum \geqslant th_{epe} \end{cases} \quad (11)$$

By checking $Dsum$ at all sample points $\{HS, VS\}$, we obtain the objective function for EPE minimization and its gradient as follows:

$$F_{epe} = \sum_{(i,j)\in HS} sig(Dsum_{i,j}) + \sum_{(i,j)\in VS} sig(Dsum_{i,j}) \quad (12)$$

$$\nabla F_{epe} = \frac{\partial F_{epe}}{\partial p(x,y)}$$
$$= \sum_{(i,j)\in HS} \frac{\partial sig(Dsum_{i,j})}{\partial p(x,y)} + \sum_{(i,j)\in VS} \frac{\partial sig(Dsum_{i,j})}{\partial p(x,y)} \quad (13)$$

The closed form of the former part of Eq. (13) can be derived as Eq. (14), similarly for the later part.

$$\sum_{(i,j)\,\in HS} \frac{\partial sig(Dsum_{i,j})}{\partial p(x,y)}$$
$$= \sum_{(i,j)\in HS} \theta_{epe}$$
$$\cdot sig(Dsum_{i,j})(1 - sig(Dsum_{i,j})) \sum_{k=j-th_{epe}}^{j+th_{epe}} \frac{\partial D_{ik}}{\partial p(x,y)} \quad (14)$$

where

$$\frac{\partial D_{ik}}{\partial p(x,y)}$$
$$= \frac{\partial (Z_{nom}(i,k) - Z_t(i,k))^2}{\partial p(x,y)}$$
$$= 2\theta_Z \theta_M$$
$$\times (Z_{nom}(i,k) - Z_t(i,k))Z_{nom}(i,k)(1 - Z_{nom}(i,k))$$
$$\times \{[M(i,k) \otimes H_{nom}^*(i,k)]H_{nom}(i-x,k-y)$$
$$\quad + [M(i,k) \otimes H_{nom}(i,k)]H_{nom}^*(i-x,k-y)\}$$
$$\times M(i,k)(1 - M(i,k)). \quad (15)$$

Here H_{nom}^* denotes the conjugate transpose of the kernel matrix H_{nom}.

Note that the complexity of the gradient calculation is proportional to the size of the sample points $|HS|+|VS|$. If the target patterns are very complicated, the sample points would increase, and so does the computational time.

3.3 Design Target Formulation Based on Image Difference

To improve the complexity of gradient calculation, we propose another objective formulation for design target optimization. The concept is to minimize the image difference (id) between the nominal image and the target image, as shown in Eq. (16).

$$F_{id} = \sum_{i=1}^{N} \sum_{j=1}^{N} (Z_{nom}(i,j) - Z_t(i,j))^{\gamma} \qquad (16)$$

where γ is used to control the weight of the impact made by the image difference. The gradient can be derived as:

$$
\begin{aligned}
\nabla F_{id} = \gamma \theta_Z \theta_M \cdot \{ & H_{nom} \\
\otimes [(Z_{nom} - Z_t)^{\gamma-1} & \odot Z_{nom} \odot (1 - Z_{nom}) \odot (M \otimes H_{nom}^*)] \\
& + H_{nom}^* \\
\otimes [(Z_{nom} - Z_t)^{\gamma-1} & \odot Z_{nom} \odot (1 - Z_{nom}) \odot (M \otimes H_{nom})] \} \\
\odot M \odot (1 - M) &
\end{aligned}
$$
$$(17)$$

The quadratic form ($\gamma = 2$) of Eq. (16) has been used in previous ILT studies. We find that when performing the co-optimization of design target and process window, setting different γ can help make a trade-off between these two objectives. In our implementation, γ is set as 4.

3.4 Co-optimization for Design Target and Process Window

PV Band is the area between the outermost printed edge and the innermost printed edge among all process conditions. However, the outermost/innermost edge may be formed by more than one process condition [20]. As illustrated in Fig. 4, the calculation of PV Band requires a series of boolean operations through all possible printed images. However, these boolean operations are difficult to model with a continuous form.

Therefore, we try to minimize the difference between possible images and the target image, as defined in Eq. (18) where N_p is the number of possible process conditions. With this formulation, we expect that inner edges and outer edges can be optimized toward the target edges which reduces the overall PV Band.

$$F_{pvb} = \sum_{k=1}^{N_p} (Z_k - Z_t)^2 \qquad (18)$$

By combining Eq. (12) and Eq. (16) with Eq. (18), we can obtain the following objective functions that optimize design target and process window simultaneously. Both of the two functions are applied into Alg. 1 as $MOSAIC_{exact}$ and $MOSAIC_{fast}$ respectively, and evaluated in Sec. 4.

$$F_{exact} = \alpha F_{epe} + \beta F_{pvb} \qquad (19)$$

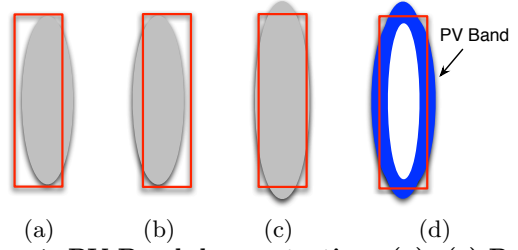$$F_{fast} = \alpha F_{id} + \beta F_{pvb} \qquad (20)$$

(a) (b) (c) (d)

Figure 4: PV Band demonstration. (a)∼(c) Printed images under different process conditions. (d) Resulted PV Band.

3.5 Speedup for Kernel Convolution

The gradient calculation requires a large amount of computational efforts from convolution operations, which is the main overhead of our approaches. We transform the non-quadratic form of Eq. (2) into Eq. (21) based on the properties of convolution, associativity with scalar multiplication and distributivity. With the new formulation of the kernel function, we can precompute H by combing all kernel models without losing the accuracy. This reduces the convolution operations by N_h times and significantly improves the efficiency of our approaches.

$$
\begin{aligned}
M \otimes H &= \sum_{k=1}^{N_h} w_k \cdot (M \otimes h_k) = \sum_{k=1}^{N_h} M \otimes (w_k \cdot h_k) \\
&= M \otimes \sum_{k=1}^{N_h} w_k \cdot h_k
\end{aligned}
$$
$$(21)$$

4. EXPERIMENTAL RESULTS

Our ILT methods are implemented in C/C++ and tested on Linux machine with 3.4 GHz CPUs and 32 GB memory. We adopt the optical parameters from [22], with 193nm wavelength, a defocus range of $\pm 25nm$ and a dose range of $\pm 2\%$. Ten benchmarks released by IBM for the ICCAD 2013 contest [22] are tested, which represent the most challenging shapes to print. Each benchmark is a layout clip of 32nm M1 layer, with a size of $1024nm \times 1024nm$. The resolution of the pixelated mask is 1nm per pixel. EPE constraint th_{epe} is set as 15nm. EPE sample points are measured every 40nm along the pattern boundaries.

The parameters α and β in our objective functions are set based on the scoring function provided in [22] as follows:

Minimize: $Score = Runtime + 4 \times PV\ Band +$
$5000 \times \#EPE\ Violation + 10000 \times ShapeViolation$
$$(22)$$

where $ShapeViolation$ is based on the existence of holes in the final contour. All our results produce zero $ShapeViolation$.

We compare our results with the top 3 winners of the ICCAD 2013 contest, where those approaches are also designed to optimize Eq. (22). The results are shown in Table 2 in terms of the number of EPE violations (#EPE), the area of process variability band (PVB), and $Score$. With the given scoring function, our approaches successfully achieve the best result (lowest score). Table 3 shows the runtime comparison of different OPC approaches. Note that the compared approaches are run on a different machine (2.65GHz CPU) from ours. However, we can still see that the runtime of MOSAIC_fast is around the same scale as the contest results. Moreover, runtime only accounts for a small portion of the overall score, which accounts 0.12% for MOSAIC_fast and 0.75% for MOSAIC_exact, respectively. Examples of our OPC result can be seen in Fig. 5.

Table 2: Comparison with the winners of the ICCAD 2013 contest.

Testcases		1st place			2nd place			3rd place			MOSAIC_fast			MOSAIC_exact		
Name	Pattern Area	#EPE	PVB	Score	#EPE	PVB	Score	#EPE	PVB	Score	#EPE	PVB	Score	#EPE	PVB	Score
B1	215344	0	65743	263578	6	57190	259242	2	70014	290329	6	58232	263246	9	56890	274267
B2	169280	1	53335	218659	13	45776	248589	0	58927	235838	10	47139	238812	4	48312	214493
B3	213504	25	143993	701266	39	90493	557459	35	106676	602009	59	82195	624101	52	84608	600955
B4	82560	0	31654	127030	14	24276	167591	1	38401	158891	1	28244	118298	3	24723	115161
B5	281958	0	65529	262378	16	55754	303505	4	69796	299394	6	56253	255327	2	56299	237363
B6	286234	1	62164	254086	18	49059	286718	0	59315	237351	1	50981	209238	1	49285	204224
B7	229149	0	51098	204787	8	43663	215134	8	56972	268241	0	46309	185475	0	46280	186761
B8	128544	0	25802	103447	0	23810	95771	0	26106	104504	2	22482	100186	2	22342	100031
B9	317581	2	74931	310008	15	62164	324225	12	78781	375533	6	65331	291646	3	62529	268138
B10	102400	0	18433	73904	0	19585	78829	0	18579	74376	0	18868	75703	0	18141	73276
Ratio			1.11			1.12			1.16			1.04			1.00	

Pattern Area/PVB unit: nm^2

Table 3: Runtime comparison with the winners of the ICCAD 2013 contest.

Testcases	1st place	2nd place	3rd place	MOSAIC_fast	MOSAIC_exact
B1	606	482	273	318	1707
B2	319	485	130	256	1245
B3	294	487	305	321	2523
B4	414	487	287	322	1269
B5	262	489	210	315	2167
B6	430	482	91	314	2084
B7	395	482	353	239	1641
B8	239	531	80	258	663
B9	284	569	409	322	3022
B10	172	489	60	231	712
Average	341.5	498.3	219.8	289.6	1703.3

unit: *second*

4.1 Convergence of Gradient Descent

We further investigate the convergence of our gradient descent based ILT. In our experiments of Alg. 1, the maximum iteration number th_{iter} is 20 and the optimization is stopped at $th_g = 0.015$. Fig. 6 shows the convergence curves of testcase B4 and B6. We can see that the number of EPE violations gradually decreases while PV Band goes the opposite. This is because EPE has higher weight in the objective function. In the first few iterations, the mask patterns are nearly non-printable, and thus the result is less stable. The patterns become printable after a few optimization procedures, which also reflects the increase of PV Band as more iterations applied. In general, the optimization can converge quite effectively within 20 iterations.

5. CONCLUSION

As the increasing challenges of semiconductor manufacturing, OPC becomes much more difficult. ILT based approaches have been a promising candidate for advanced technology nodes. We propose new mask optimizing solutions considering design target and process window simultaneously. Two approaches, MOSAIC_exact based on exact EPE minimization and MOSAIC_fast with efficient gradient computation are tested on 32nm designs. The results show that both of our approaches outperform the winners of the IC-CAD 2013 contest.

6. ACKNOWLEDGMENT

7. REFERENCES

[1] A. K. Wong. Resolution enhancement techniques. *SPIE Press*, 2001.

[2] N. B. Cobb and Y. Granik. OPC methods to improve image slope and process window. In *Proc. of SPIE*, 2003.

[3] P. Yu and D. Z. Pan. TIP-OPC: a new topological invariant paradigm for pixel based optical proximity correction. In *Proc. Int. Conf. on Computer Aided Design*, 2007.

[4] Y. Granik. Illuminator optimization methods in microlithography. In *Proc. of SPIE*, volume 5754, 2005.

[5] L. Pang, Y. Liu, and D. Abrams. Inverse lithography technology (ILT): What is the impact to the photomask industry? In *Proc. of SPIE*, volume 6283, 2006.

[6] Guangming Xiao, Dong Hwan Son, Tom Cecil, Dave Irby, David Kim, Ki-Ho Baik, Byung-Gook Kim, SungGon Jung, Sung Soo Suh, and HanKu Cho. E-beam writing time improvement for inverse lithography technology mask for full-chip. In *Proc. of SPIE*, volume 7748, 2010.

[7] Y. Granik. Fast pixel-based mask optimization for inverse lithography. *Journal of Micro/Nanolithography, MEMS, and MOEMS*, 5(4), 2006.

[8] Y. Shen, N. Wong, and E. Y. Lam. Level-set-based inverse lithography for photomask synthesis. *Optics Express*, 17(26), 2009.

[9] A. Poonawala and P. Milanfar. Mask design for optical microlithography mdash;An inverse imaging problem. *IEEE Trans. on Computer-Aided Design of Integrated Circuits and Systems*, 16(3), 2007.

[10] X. Ma and G. R. Arce. Generalized inverse lithography methods for phase-shifting mask design. In *Optics Express*, volume 15, 2007.

[11] N. Jia and E. Y. Lam. Machine learning for inverse lithography: using stochastic gradient descent for robust photomask synthesis. *Journal of Optics*, 12(4), 2010.

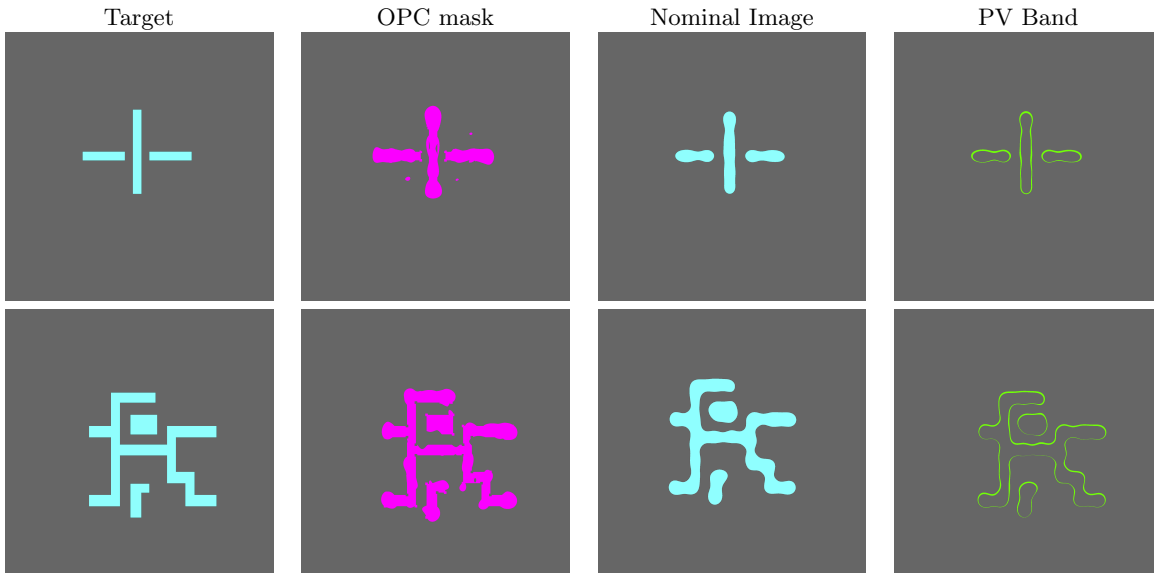[12] X. Zhao and C. Chu. Line search-based inverse lithography

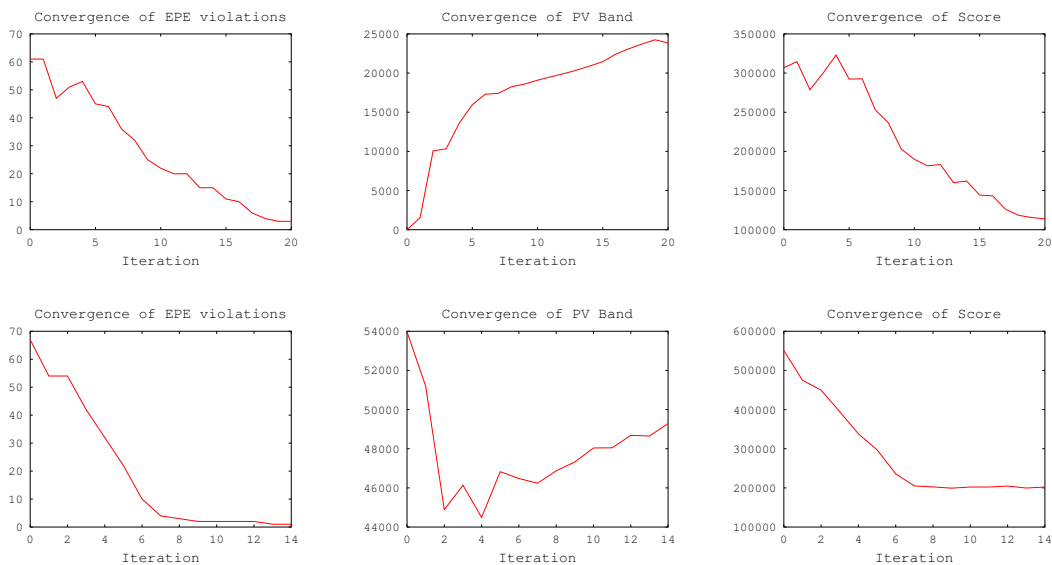Figure 5: OPC result examples with MOSAIC_exact. First row: B4; second row: B6.

Figure 6: Convergence of the gradient decent with MOSAIC_exact. First row: B4; second row: B6.

technique for mask design. *Proc. Int. Conf. on VLSI Design*, 2012.

[13] Jinyu Zhang, Wei Xiong, Yan Wang, and Zhiping Yu. A highly efficient optimization algorithm for pixel manipulation in inverse lithography technique. In *Proc. Int. Conf. on Computer Aided Design*, November 2008.

[14] Jinyu Zhang, Wei Xiong, Yan Wang, Zhiping Yu, and Min-Chun Tsai. A robust pixel-based RET optimization algorithm independent of initial conditions. In *Proc. Asia and South Pacific Design Automation Conf.*, January 2010.

[15] A. Krasnoperova, J. A. Culp, I. Graur, S. Mansfield, M. Al-Imam, and H. Maaty. Process window OPC for reduced process variability and enhanced yield. In *Proc. of SPIE*, volume 6154, 2006.

[16] P.Yu, S.X. Shi, and D. Z. Pan. True process variation aware optical proximity correction with variational lithography modeling and model calibration. *Journal of Micro/Nanolithography, MEMS, and MOEMS*, 6(3), 2007.

[17] S. Banerjee, K. B. Agarwal, and M. Orshansky. Methods for joint optimization of mask and design targets for improving lithographic process window. *Journal of Micro/Nanolithography, MEMS, and MOEMS*, 12(2), 2013.

[18] H. Hopkins. The concept of partial coherence in optics. Proceedings of the Royal Society of London, 1953.

[19] N. Cobb. Fast optical and process proximity correction algorithms for integrated circuit manufacturing. *PhD dissertation, University of California at Berkeley*, 1998.

[20] J. A. Torres and C. N. Berglund. Integrated circuit DFM framework for deep subwavelength processes. In *Proc. of SPIE*, volume 5756, 2005.

[21] X. Ma and G. R. Arce. *Computational Lithography*. Wiley Series in Pure and Applied Optics, first edition, 2010.

[22] ICCAD contest 2013 [http://cad_contest.cs.nctu.edu.tw/CAD-contest-at-ICCAD2013/problem_c/].